L. Kumaresan, M. Mahalakshmi, M. Palanichamy, and V. Murugesan, 'Synthesis, Characterization, and Photocatalytic Activity of Sr2+ Doped TiO2 Nanoplates'. Ind. Eng. Chem. Res. (49,...

ARTICLE *in* INDUSTRIAL & ENGINEERING CHEMISTRY RESEARCH · JANUARY 2010

Impact Factor: 2.59

Synthesis, Characterization, and Photocatalytic Activity of Sr^{2+} Doped TiO_2 Nanoplates

L. Kumaresan,[†] M. Mahalakshmi,[‡] M. Palanichamy,[†] and V. Murugesan*[,†]

Department of Chemistry, Anna University, Chennai 600 025, India, and Department of Chemistry, SSN College of Engineering, Kalavakkam 603 110, India

Strontium doped titania (TiO_2) nanoplates and titania nanoparticles were synthesized by sol−gel method. The characterization of the materials revealed the mesoporous nanoplate-like structure for Sr^{2+} doped TiO_2. The thickness and edge length of Sr^{2+} doped TiO_2 nanoplates were found to be 12 nm and 25−75 nm, respectively. TiO_2 nanoparticles and Sr^{2+} doped TiO_2 nanoplates showed higher surface area due to the presence of mesopores. The photocatalytic activity of TiO_2 nanoparticles and Sr^{2+} doped TiO_2 nanoplates was evaluated using 2,4-dinitrophenol (DNP) as a model pollutant. The photocatalytic activity of Sr^{2+} doped TiO_2 nanoplates was higher than both TiO_2 nanoparticles and commercial TiO_2 (Degussa P-25). Sr^{2+} doped TiO_2 nanoplates exhibited enhanced photocatalytic activity due to increases in the band gap energy and surface area.

1. Introduction

TiO_2, as a photocatalyst, has become the focus of numerous studies due to its attractive characteristics and application in the remediation of environmental contaminants.[1] Despite its potential application, the fast recombination of photogenerated electron−hole pair on the surface or in the lattice of TiO_2 hinders its commercialization.[2] Doping of metal ions in TiO_2 is the latest technique to suppress the rate of recombination of electron−hole pair. Doping of a metal ion in a semiconductor is known to affect both photophysical behavior and photochemical activity. Enhanced photocatalytic activity over binary metal oxides and transition metal doped TiO_2 was reported by Choi et al.[3] and Anderson and Bard.[4] Transition metal ion doping improved the trapping of electrons and inhibited the electron−hole recombination.[5] Noble metal ion doping in semiconductors promoted separation of photogenerated charge carriers and improved the photocatalytic activity.[6] The rare earth metal ion doped TiO_2 nanoparticles were reported to exhibit higher photocatalytic activity due to efficient charge separation.[7−9]

Acceptor-doped perovskite-type oxides involving alkaline earth metals such as Ca, Sr, and Ba absorb visible light. Such acceptor-doped perovskite-type oxides are known as p-type semiconductors.[10] The composite powders having the junctions of n-type TiO_2 with p-type oxides exert higher photocatalytic activity than pristine TiO_2 particles. The conduction band minimum and the valence band maximum in the alkaline earth titanates are nearly equal to those in TiO_2.[11] Strontium titanate has been known to possess photocatalytic activity.[12,13] Wang et al.[14] reported that nitrogen doped $SrTiO_3$ exhibited higher photocatalytic activity than $SrTiO_3$. Cr^{3+} doped $SrTiO_3$ showed higher activity in the evolution of H_2.[15] In the present study, strontium doped TiO_2 nanoparticles with platelike structure were prepared by acetic acid hydrolyzed sol−gel method using titanium tetraisopropoxide and strontium nitrate as precursors for Ti and Sr, respectively. The photocatalytic activity of Sr^{2+} doped TiO_2 nanoplates was evaluated using 2,4-dinitrophenol (2,4-DNP) as the model pollutant.

* To whom correspondence should be addressed. Tel.: +91-44-22203144. Fax: +91-44-22200889. E-mail: v_murugu@hotmail.com.
[†] Anna University.
[‡] SSN College of Engineering.

2. Materials and Methods

2.1. Materials. Titanium tetraisopropoxide, $Ti[OCH(CH_3)_2]_4$ (Merck) and strontium nitrate $Sr(NO_3)_2 \cdot 6H_2O$ (CDH) were used for the preparation of Sr^{2+} doped TiO_2 nanoplates. Glacial acetic acid, CH_3COOH (SRL Ltd.), and 2,4-dinitrophenol (2,4-DNP), $C_6H_4N_2O_5$ (SRL), were used as such. Double distilled water was used for the preparation of all solutions.

2.2. Catalyst Preparation. The typical sol−gel synthesis of Sr^{2+} doped TiO_2 nanoplates is as detailed below. Titanium tetraisopropoxide (14.3 mL) was mixed with glacial acetic acid (28 mL), and the solution was kept undisturbed for 10 min to get a homogeneous mixture. A stoichiometric amount of strontium nitrate in 150 mL of water was added to the mixture under vigorous stirring to obtain the required concentration. Titanium tetraisopropoxide, glacial acetic acid, and water were maintained in the molar ratio 1:10:300. When the resulting mixture turned to be a sol, it was stirred for 5 h and aged for 2 days to form a gel. The gel was dried in vacuum at 70 °C for 24 h and then in an oven at 100 °C for 24 h and finally ground. The resulting powder was calcined at 500 °C for 5 h. The doping concentrations of Sr are expressed as weight percent.

2.3. Catalyst Characterization. The X-ray diffraction (XRD) patterns of TiO_2 nanoparticles and Sr^{2+} doped TiO_2 nanoplates were recorded on a PANalytical X'Pert Pro X-ray diffractometer using Cu Kα radiation as the X-ray source. The diffractograms were recorded in the 2θ range of 10−80° in steps of 0.02° with a count time of 20 s at each point. The particle size was determined from the broadening of the diffraction peak using the Scherrer formula, $D = K\lambda/\beta \cos \theta$, where D is the crystallite size (nm), K is the Scherrer constant, λ is the wavelength of the X-ray source, β is the full width at half-maximum, and θ is the Bragg angle. Transmission electron microscopic (TEM) images were recorded using a JEOL TEM-3010 electron microscope operating at an accelerating voltage of 300 keV. Scanning electron microscopy (SEM) pictures were recorded using a scanning electron microscope with energy dispersive X-ray spectrometer (SEM-EDX; Leo Stereoscan 440). The surface area of nano-TiO_2 and Sr^{2+} doped TiO_2 nanoplates was measured with Quantochrome Autosorb 1 sorption analyzer using nitrogen as adsorbent at 77 K. Prior to the analysis, the samples were degassed for 3 h at 250 °C under vacuum (10^{-5} mbar) in the degas port of the adsorption analyzer. FT-IR spectra

10.1021/ie901191z
Published on Web 01/12/2010

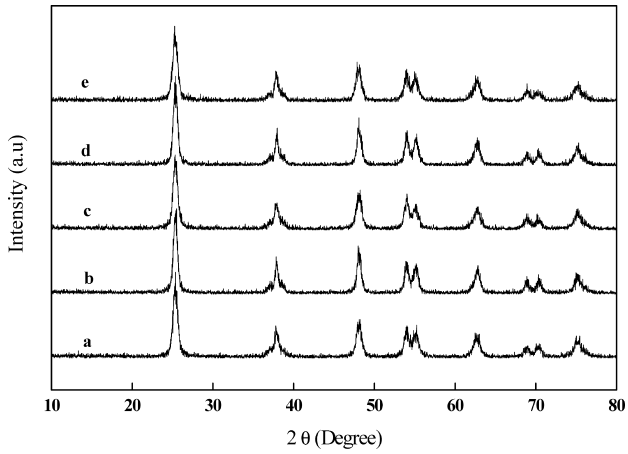

Figure 1. XRD patterns of (a) TiO_2 nanoparticles, (b) 0.05 wt % Sr^{2+} doped TiO_2, (c) 0.1 wt % Sr^{2+} doped TiO_2, (d) 0.3 wt % Sr^{2+} doped TiO_2, (e) 0.5 wt % Sr^{2+} doped TiO_2, and (f) 1.0 wt % Sr^{2+} doped TiO_2.

were recorded using a FT-IR spectrometer (Nicolet Avator 360). UV−vis absorption spectra of the synthesized materials were recorded in a spectrophotometer (Shimadzu UV-2101) equipped with an integrating sphere.

2.4. Photocatalytic Degradation Studies and Analysis. Photocatalytic degradation of 2,4-DNP was performed in an aqueous medium in a slurry batch reactor. A cylindrical photochemical reactor of 30 × 2 cm (height × diameter), provided with a water circulation arrangement to maintain the temperature in the range of 25−30 °C, was used in all the experiments. The UV irradiation was carried out using 8 × 8 W low-pressure mercury lamps built into a lamp housing with polished anodized aluminum reflectors placed 12 cm away from the reactor. These lamps emit predominantly UV radiation at a wavelength of 254 nm and another 8 lamps were arranged alternatively to emit UV radiation at a wavelength of 365 nm. The reactor setup was covered with aluminum foil followed by a black cloth to prevent UV light leakage. 2,4-DNP stock solution containing 300 mg L^{-1} was prepared in double distilled water and diluted to the required concentration. In a typical procedure, 100 mg of the catalyst was added to 100 mL 2,4-DNP solution of 200 mg L^{-1} and the resultant slurry was stirred for 30 min to attain equilibrium. It was then irradiated with UV light of either 254 or 365 nm with continuous purging of air free from CO_2.

Aliquots were withdrawn at specific time intervals and analyzed after centrifugation followed by filtration with 0.2 μm membrane to remove the catalyst particles. The change in the concentration of 2,4-DNP was measured from its characteristic absorption band using UV−visible spectrophotometer (Shimadzu model 1601). The extent of degradation and formation of intermediates were monitored using high-performance liquid chromatograph (HPLC; Shimadzu, LC-10 ATvp pump and SPD-10Avp UV−visible detector adjustable to 210 and 270 nm with reverse-phase ODS column). The mobile phase in the HPLC is composed of acetonitrile and triple distilled water (60:40 (v/v)). The extent of mineralization of 2,4-DNP was followed by using a total organic carbon analyzer (TOC; Shimadzu TOC-V CPN).

3. Results and Discussion

3.1. Catalyst Characterization. The XRD patterns of TiO_2 nanoparticles and Sr^{2+} doped TiO_2 nanoplates are shown in Figure 1. The sharp intense peak at $2\theta = 25.3$ corresponds to anatase (101) phase. The particle size of Sr^{2+} doped TiO_2 calculated using the Scherrer equation was found to be 12 nm. Separate peaks for $SrTiO_3$ or Sr−O were not observed due to low dopant concentration, as reported earlier.[16] The doping of Sr^{2+} stabilizes the anatase phase without its conversion to rutile phase. It is difficult for Sr^{2+} ion to enter the lattice of TiO_2 as its ionic radius is too high (1.12 Å) compared to Ti^{4+}. It is difficult to predict whether Sr^{2+} exists as Sr−O on the surface of TiO_2 or as $SrTiO_3$ from the XRD patterns due to low dopant concentration.

The TEM image of 0.1 wt % Sr^{2+} doped TiO_2 is shown in Figure 2a. The TEM image clearly indicates that Sr^{2+} doped TiO_2 nanoplates possess an average width of 12 nm and length of 25−75 nm. The TEM image of TiO_2 nanoparticles clearly shows the spherical shape of TiO_2 nanoparticles (Figure 3a) with the particle size distribution in the range of 5−12 nm. The magnified images of Sr^{2+} doped TiO_2 nanoplates and TiO_2 nanoparticles (Figures 2b and 3b) showed the lattice fringes of TiO_2 nanoparticles. Ueda and Matsuo[11] reported that the addition of strontium contributes to the elongated platelike morphology with appropriate surface orientation, which may act as a photocatalytic electrode with the large potential gradient. The platelike morphology with a well-developed plane (001) for $Sr_3Ti_2O_7$ of the Ruddlesden−Popper type crystal structure was

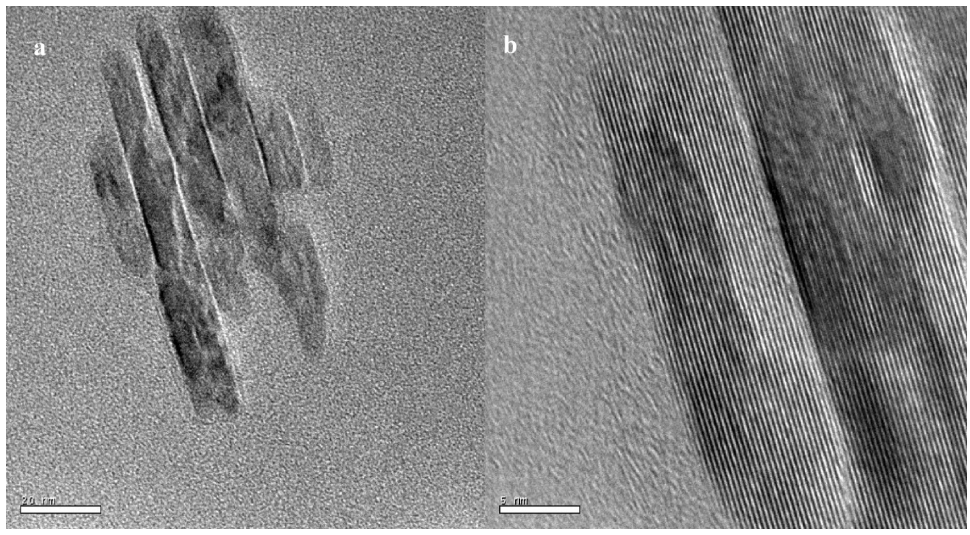

Figure 2. TEM micrographs of (a) 0.1 wt % Sr^{2+} doped TiO_2 nanoplates in a scale bar of 20 nm and (b) magnified image of 0.1 wt % Sr^{2+} doped TiO_2 nanoplates in the scale bar of 5 nm.

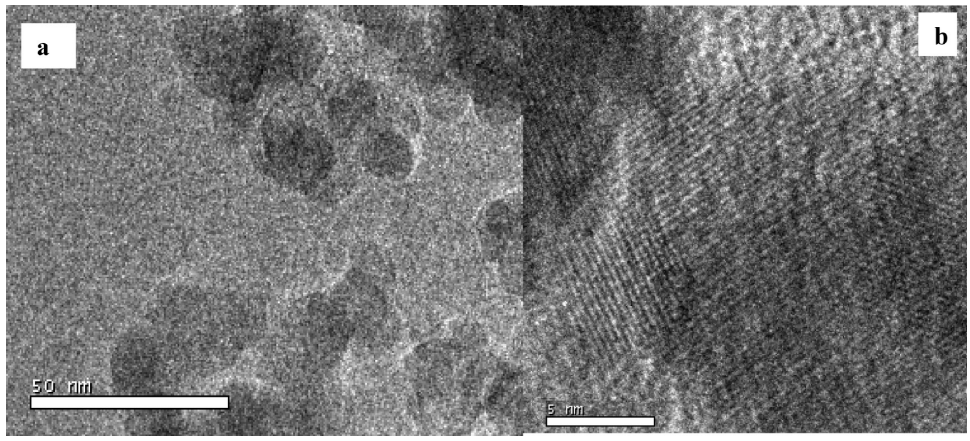

Figure 3. TEM micrographs of (a) TiO_2 nanoparticles and (b) magnified image of TiO_2 nanoparticles.

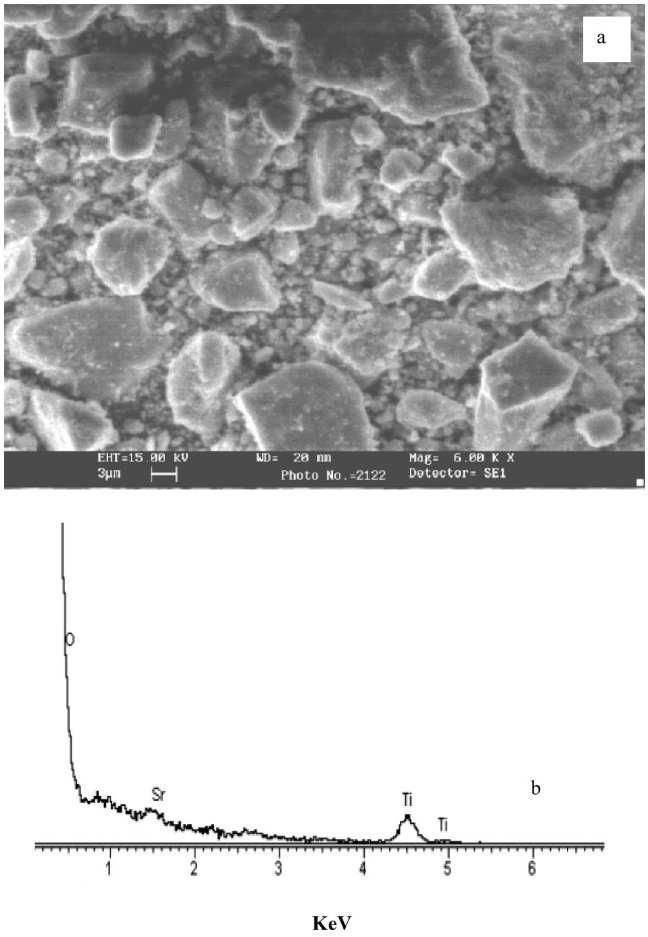

Figure 4. SEM micrographs of (a) 0.1 wt % of Sr^{2+} doped TiO_2 and (b) EDX of 0.1 wt % Sr^{2+} doped TiO_2.

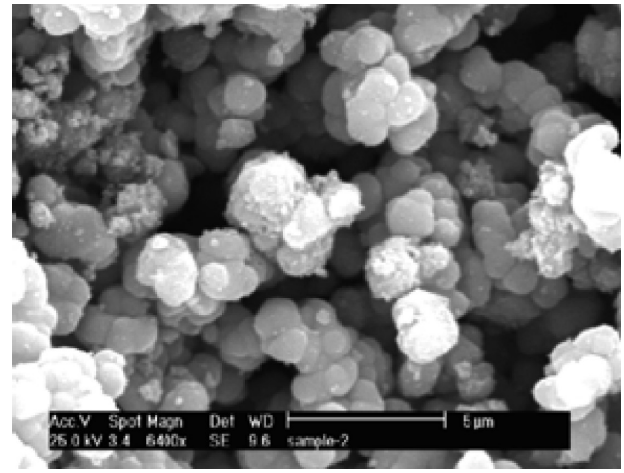

Figure 5. SEM micrograph of TiO_2 nanoparticles.

reported by Takeuchi et al.[17] The scanning tunneling microscopic (STM) pictures of $SrTiO_3$ as reported by Kubo and Nozoye[18] and Sudhoh and Iwasaki[19] showed a similar type of shape composed of large terraces.

The SEM image of 0.1 wt % Sr^{2+} doped TiO_2 is shown in Figure 4a. There is uneven distribution of agglomerated particles. However, growth of plates with a smooth terrace is evident. Adsorbed grains elongating on the sides of the plates are also seen. SEM images of pristine TiO_2 nanoparticles synthesized by the same sol−gel process exhibit a uniform spherical shape (Figure 5). However, defective terrace as a result of agglomeration of tiny grains is not seen in these SEM images. Strontium doping in TiO_2 is clearly identified from the EDX image of 0.1 wt % Sr^{2+} doped TiO_2 in Figure 4b.

The TEM and SEM images clearly reveal that the added Sr^{2+} is expected to influence the morphology of TiO_2 significantly. Therefore the platelike growth that occurred by the addition of Sr^{2+} to the growing crystal is in a systematic manner. It is evident that Sr^{2+} doping perturbed the TiO_2 morphology. With an ionic radius of 0.113 nm, the size misfit due to strontium substitution in the titanium site ($r = 0.068$ nm) served as a more efficient misfit dopant. Ling and Yan[20] reported that strontium segregates to the grain boundaries to form a continuous second phase between 1250 and 1400 °C. Growth of $SrTiO_3$ as a second phase probably begins between 1200 and 1250 °C. Below 1200 °C, this continuous second phase breaks up into discrete particles with length generally several times greater than its width. Since the annealing temperature in this study was low, strontium segregating to the grain boundaries induced the formation of elongated nanoplates.

The specific surface area, pore volume, and pore size of TiO_2 (Degussa P-25), TiO_2 nanoparticles, and Sr^{2+} doped TiO_2 nanoplates are presented in Table 1. The surface area of TiO_2 (Degussa P-25) is lower than that of nano-TiO_2, due to mesopores formed in the latter. Because of the nanosize and associated high surface free energy, the particles are organized by Lewis acid base interaction to form mesopores. The enhanced surface area of 0.1 wt % Sr^{2+} doped TiO_2 compared to nanosized TiO_2 is due to its increase in the mesopore size and mesopore volume. Thus, Sr^{2+} is visualized to exhibit the role of enhancing mesopore formation by

Table 1. Specific Surface Area, Pore Volume, and Pore Size of TiO_2(Degussa P-25), TiO_2 Nanoparticles, and Sr^{2+} Doped TiO_2 Nanoplates

catalyst	specific surface area ($m^2\ g^{-1}$)	pore volume ($cm^3\ g^{-1}$)	pore size (Å)
TiO_2 (Degussa P-25)	50		
TiO_2 nanoparticles	66	0.209	37
0.1 wt % Sr^{2+} doped TiO_2 nanoplates	104	0.303	43
0.3 wt % Sr^{2+} doped TiO_2 nanoplates	97	0.302	47
0.5 wt % Sr^{2+} doped TiO_2 nanoplates	83	0.246	44

organizing nanosized TiO_2 particles. The formation of hysteresis loop in the plot of relative pressure vs volume of N_2 adsorbed supports the presence of mesopores in both Sr^{2+} doped TiO_2 nanoplates and TiO_2 nanoparticles (Figure 6a,b). The pore size distribution curves of 0.1 wt % Sr^{2+} doped TiO_2 nanoplates and TiO_2 nanoparticles are shown in Figure 7a,b. The results revealed that doping of Sr^{2+} had the influence of enlarging the pore size. Sr−O can bridge and organize the particles by Lewis acid base interaction and ultimately aid the formation mesopores. But the surface area of 0.3 wt % Sr^{2+} doped TiO_2 is slightly lower than that of 0.1 wt % Sr^{2+} doped TiO_2. However the pore volume is decreased by 0.01 unit, and pore size is increased by 4 Å; thus, the difference is not significant. But 0.5 wt % Sr^{2+} doped TiO_2 showed a significant decrease in the surface area compared to both 0.1 and 0.3 wt % Sr^{2+} doped TiO_2. The pore volume also decreased significantly, but the pore size decreased only by 3 Å. So, the main role of Sr^{2+} to construct mesopore is

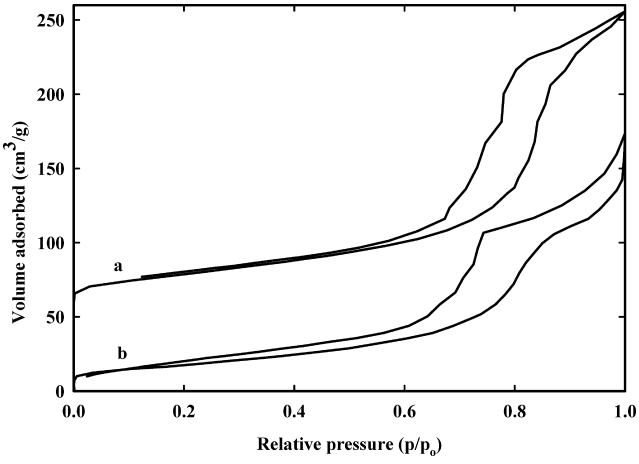

Figure 6. Nitrogen adsorption−desorption isotherms for (a) 0.1 wt % Sr^{2+} doped TiO_2 and (b) TiO_2 nanoparticles.

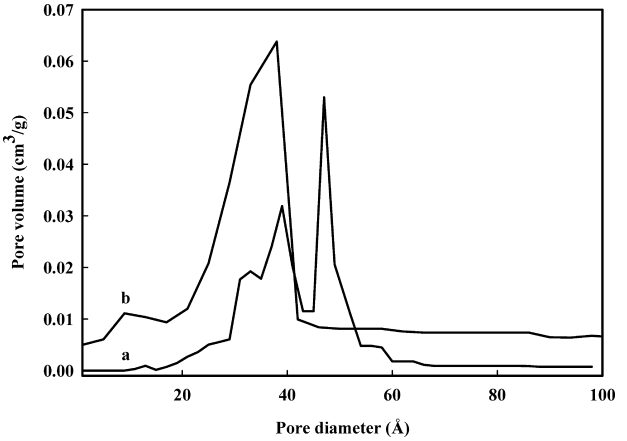

Figure 7. Pore size distribution of (a) 0.1 wt % Sr^{2+} doped TiO_2 and (b) TiO_2 nanoparticles.

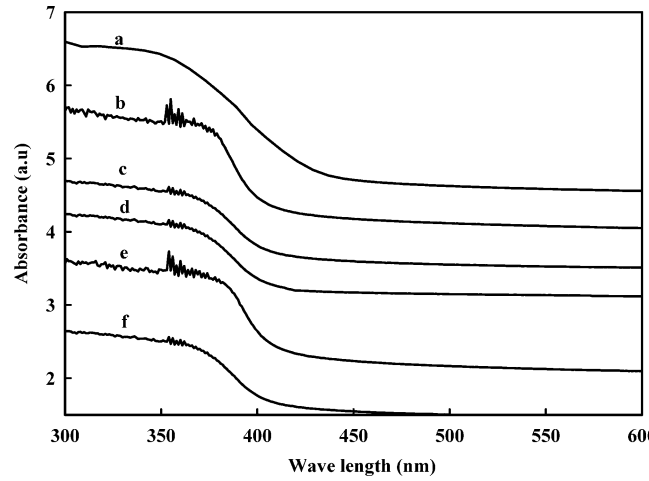

Figure 8. UV−vis absorption spectra of (a) TiO_2 nanoparticles, (b) 0.05 wt % Sr^{2+} doped TiO_2, (c) 0.1 wt % Sr^{2+} doped TiO_2, (d) 0.3 wt % Sr^{2+} doped TiO_2, (e) 0.5 wt % Sr^{2+} doped TiO_2, and (f) 1.0 wt % Sr^{2+} doped TiO_2.

still retained, but its high content facilitates large growth in particle size to form a platelike structure, as discussed in SEM analysis. Therefore, the high content of Sr^{2+} is predicted to aid growth in all three dimensions, as the particle surface could be planted with Sr^{2+} on all sides. The TEM pictures support this view. Hence, the optimum amount of loading was found to be 0.1 wt %.

UV−vis absorption spectral analysis is used to probe the band structure of materials. UV−vis absorption spectra of TiO_2 nanoparticles and Sr^{2+} doped TiO_2 nanoplates are shown in Figure 8. The absorbance of Sr^{2+} doped TiO_2 nanoplates is shifted toward shorter wavelength than TiO_2 nanoparticles. Sr^{2+} doped TiO_2 nanoplates gave absorbance at 386 nm and TiO_2 nanoparticles at 398.5 nm in the electronic spectra. The band gap values calculated for these absorbance values are 3.21 and 3.11 eV, respectively. Zhou et al.[21] reported the band gap energy of TiO_2 (Degussa P-25) as 3.08 eV. All of the prepared Sr^{2+} doped TiO_2 nanoplates show higher band gap energy than TiO_2 nanoparticles and TiO_2 (Degussa P-25). But an increase of Sr^{2+} doping beyond 0.1 wt % shows a shift toward longer wavelength due to an increase of the particle size. The large band gap is important in preventing the electron−hole recombination and ultimately enhances the photocatalytic activity.

FT-IR spectra of nano-TiO_2 and Sr^{2+} doped TiO_2 nanoplates are shown in Figure 9. In the spectrum of pure TiO_2 nanoparticles, the Ti−O vibration gives an intense, broadband between 1000 and 400 cm^{-1}. The surface water of TiO_2 nanoparticles gives a broad envelope around 3400 cm^{-1}. The presence of surface water is again confirmed by its bending mode at 1630 cm^{-1}. Similar patterns are also shown by the spectra of Sr^{2+} doped nanoplates. Sr−O vibration was reported to occur at 200 cm^{-1}.[22] The spectra presented in Figure 9 are recorded between 400 and 4000 cm^{-1}, wherein the Sr−O vibration is not shown. The peak maximum close to 480 cm^{-1} is shifted to higher energy in all the spectra of Sr^{2+} doped TiO_2 nanoplates, and this is taken as evidence for Sr^{2+} interaction with TiO_2.

3.2. Evaluation of Photocatalytic Activity of Sr^{2+} Doped TiO_2 Nanoplates. The efficiency of photocatalytic activity of Sr^{2+} doped TiO_2 nanoplates was investigated by following the mineralization of 2,4-DNP under optimized experimental conditions. The results reveal that the photocatalytic activity of 0.1 wt % Sr^{2+} doped TiO_2 is higher than TiO_2 nanoparticles and commercial TiO_2 (Degussa P-25; Figure 10). There is no

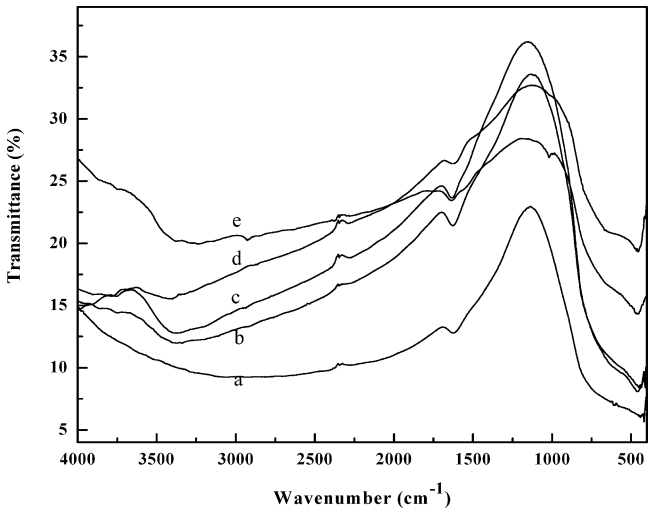

Figure 9. FT-IR spectra of (a) TiO_2 nanoparticles, (b) 0.05 wt % Sr^{2+} doped TiO_2, (c) 0.1 wt % Sr^{2+} doped TiO_2, (d) 0.3 wt % Sr^{2+} doped TiO_2, and (e) 0.5 wt % Sr^{2+} doped TiO_2.

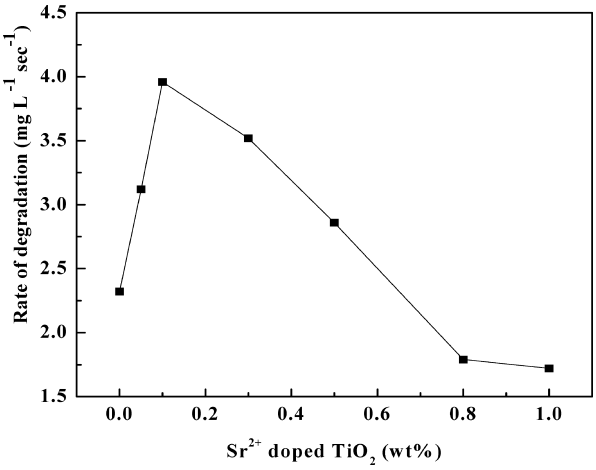

Figure 10. Rate of degradation of 2,4-DNP with different weight percents of Sr^{2+} doped TiO_2 nanoplates.

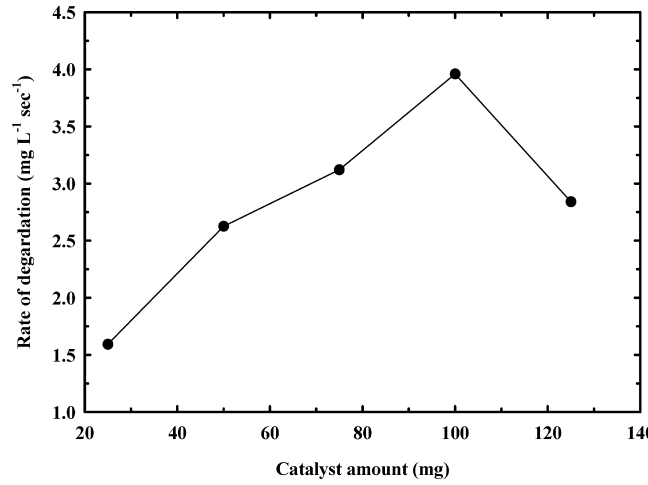

Figure 11. Rate of degradation of 2,4-DNP with different amounts of 0.1 wt % Sr^{2+} doped TiO_2 nanoplates.

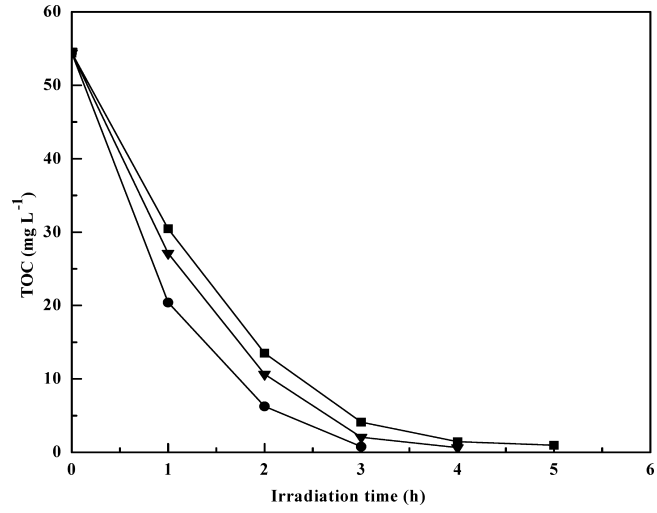

Figure 12. Photocatalytic mineralization of 2,4-DNP using (■) TiO_2 nanoparticles, (▼) 0.1 wt % Sr^{2+} doped TiO_2 nanoplates, and (●) TiO_2 (Degussa P-25).

significant change in the activity for other weight percent Sr^{2+} doped TiO_2 catalysts. However, the activity slightly decreases with an increase in the weight percent of the Sr^{2+} content in TiO_2. This slight decrease in the activity is attributed to a small decreasing trend in the surface area of the catalyst while going from 0.1 to 1.0 wt % Sr^{2+} doped TiO_2. Among the Sr^{2+} doped TiO_2 nanoplates, 0.1 wt % Sr^{2+} doped TiO_2 demonstrates the highest photocatalytic activity due to its high surface area. Since the band gap energy is high, the rate of recombination of the electron−hole pair decreases. The photocatalytic activity of Sr^{2+} doped TiO_2 nanoplates is higher with light of wavelength 254 nm than that of 365 nm for 2,4-DNP because the absorbance for Sr^{2+} doped TiO_2 nanoplates has been shifted toward shorter wavelength due to its high band gap energy compared to that of TiO_2 nanoparticles. The rate of degradation of 2,4-DNP with different amounts of 0.1 wt % Sr^{2+} doped TiO_2 nanoplates is shown in Figure 11. It is evident that the rate of photodegradation increases linearly with catalyst loading up to 100 mg/(100 mL). Above this loading, the decrease in rate was observed due to the increase in turbidity of the solution, which reduced the light transmission through the solution. While below this level, the catalyst surface and absorption of light by the catalyst are the limiting factors. The increased loading of catalyst increases the quantity of photons absorbed and consequently the degradation rate.[23]

3.3. Photocatalytic Mineralization of 2,4-DNP Using Sr^{2+} Doped TiO_2 Nanoplates. The results of mineralization of 2,4-DNP using Sr^{2+} doped TiO_2 nanoplates are illustrated in Figure 12. As the irradiation time increased, 2,4-DNP degraded into small fragments and subsequently mineralized completely. Sr^{2+} doped TiO_2 nanoplates required lesser irradiation time than TiO_2 nanoparticles. Sr^{2+} doped TiO_2 showed enhanced photocatalytic activity due to its large band gap energy, which not only suppressed the electron−hole recombination but also generated more $^{\bullet}OH$ radicals. Since the ionic radius of Ti^{4+} is smaller than Sr^{2+}, Ti^{4+} ion replaces Sr^{2+} ion from the Sr−O lattice. To satisfy the charge imbalance, hydroxide ions could be adsorbed on the surface and the OH^- ions on the surface could accept photogenerated holes to form hydroxyl radicals and hence photoinduced charge carrier recombination is suppressed. These hydroxyl radicals are effectively used in the photodegradation.

The initial total organic carbon (TOC) value of 2,4-DNP is 56 mg L^{-1}. During the first 1 h irradiation slow mineralization was observed. This may be due to the formation of intermediates by hydroxylation of 2,4-DNP. Sr^{2+} doped TiO_2 nanoplates required 3 h for the complete mineralization of 2,4-DNP,

whereas TiO_2 nanoparticles and TiO_2 (Degussa P-25) required 4 and 5 h, respectively. Thus, Sr^{2+} doped TiO_2 nanoplates showed more enhanced activity than TiO_2 nanoparticles and TiO_2 (Degussa P-25).

4. Conclusions

TiO_2 nanoparticles and Sr^{2+} doped TiO_2 nanoplates can be conveniently prepared by sol−gel method. The physicochemical characterization revealed the morphology and particle size of these nanoparticles. This study also evidenced the misfit of strontium dopant which segregated to the grain boundaries to form a continuous second phase. This may be the reason for the formation of elongated nanoplates. TiO_2 nanoparticles proved to be better photocatalyst than commercial TiO_2 (Degussa P-25) due to increased band gap and generation of more $^{\bullet}OH$ radicals. However, Sr^{2+} doped TiO_2 nanoplates showed more enhanced activity than TiO_2 nanoparticles. The increase in the band gap led to efficient charge separation, decreased the rate of recombination of the electron−hole pair, and enhanced the rapid electron transfer at the solid−liquid interface. Since Ti^{4+} ion replaced Sr^{2+} ion from Sr−O lattice to satisfy the charge imbalance, hydroxide ions could be adsorbed on the surface and the OH^- ions on the surface could accept the photogenerated holes to form hydroxyl radicals, and hence photoinduced charge carrier recombination is suppressed. In addition, the tendency of nanoparticles to form mesopores with high surface area is also advantageous as it aids both adsorption and degradation of pollutants. Among Sr^{2+} doped TiO_2 catalysts, 0.1 wt % Sr^{2+} doped TiO_2 exhibited higher photocatalytic activity than others in the degradation of 2,4-DNP with light of wavelength 254 nm.

Acknowledgment

The authors gratefully acknowledge the University Grants Commission (UGC), New Delhi, for liberal funding in the second phase of the Centre with Potential for Excellence in Environmental Sciences (CPEES) in Anna University. The authors are also thankful to DST under FIST programme for creating the infrastructural facilities. L.K. is thankful to CSIR, New Delhi, for the award of a senior research fellowship (SRF).

Literature Cited

(1) Fujishima, A.; Rao, T. N.; Tryk, A. D. Titanium dioxide photocatalysis. *J. Photochem. Photobiol., C* **2000**, *1*, 1–21.

(2) Hoffmann, M. R.; Martin, S. T.; Choi, W.; Bahnemann, D. W. Environmental applications of semiconductor photocatalysis. *Chem. Rev.* **1995**, *95*, 69–96.

(3) Choi, W.; Termin, A.; Hoffmann, M. R. The role of metal ion dopants in quantum-sized TiO_2: Correlation between photoreactivity and charge carrier recombination dynamics. *J. Phys. Chem.* **1994**, *98*, 13669–13679.

(4) Anderson, C.; Bard, A. Improved photocatalytic activity and characterization of mixed TiO_2/SiO_2 and TiO_2/Al_2O_3 materials. *J. Phys. Chem. B* **1997**, *101*, 2611–2616.

(5) Paola, A. D.; Lopez, E. G.; Ikeda, S.; Marci, G.; Ohtani, B.; Palmisano, L. Photocatalytic degradation of organic compounds in aqueous systems by transition metal doped polycrystalline TiO_2. *Catal. Today* **2002**, *75*, 87–93.

(6) Arabatzis, I. M.; Stergiopoulos, T.; Andreeva, D.; Kitova, S.; Neophytides, S. G.; Falaras, P. Characterization and photocatalytic activity of Au/TiO_2 thin films for azo-dye degradation. *J. Catal.* **2003**, *220*, 127–135.

(7) Lin, J.; Yu, J. C. An investigation on photocatalytic activities of mixed TiO_2-rare earth oxides for the oxidation of acetone in air. *J. Photchem. Photobiol. A* **1998**, *116*, 63–67.

(8) Wang, Y.; Cheng, H.; Zhang, L.; Hao, Y.; Ma, J.; Xu, B.; Li, W. The preparation, characterization, photoelectrochemical and photocatalytic properties of lanthanide metal-ion-doped TiO_2 nanoparticles. *J. Mol. Catal. A: Chem.* **2000**, *151*, 205–216.

(9) Liqiang, J.; Xiaojun, S.; Baifu, X.; Baiqi, W.; Weimin, C.; Honggang, F. The preparation and characterization of La doped TiO_2 nanoparticles and their photocatalytic activity. *J. Solid State Chem.* **2004**, *177*, 3375–3382.

(10) Omata, T.; Matsuo, S. O. Y. Photocatalytic behavior of titanium oxide-perovskite type $Sr(Zr_{1-x}Y_x)O_{3-\delta}$ composite particles. *J. Photochem. Photobiol., A* **2003**, *156*, 243–248.

(11) Ueda, M.; Matsuo, S. O. Y. Preparation of tabular TiO_2-$SrTiO_{3-\delta}$ composite for photocatalytic electrode. *Sci. Technol. Adv. Mater.* **2004**, *5*, 187–193.

(12) Domen, K.; Kudo, A.; Onishi, T.; Kosugi, N.; Kuroda, H. Photocatalytic decomposition of water into hydrogen and oxygen over nickel(II) oxide-strontium titanate ($SrTiO_3$) powder. 1. Structure of the catalysts. *J. Phys. Chem.* **1986**, *90*, 292–295.

(13) Ahuja, S.; Kutty, T. R. N. Nanoparticles of $SrTiO_3$ prepared by gel to crystallite conversion and their photocatalytic activity in the mineralization of phenol. *J. Photochem. Photobiol., A* **1996**, *97*, 99–107.

(14) Wang, J.; Yin, S.; Komatsu, M.; Zhang, Q.; Saito, F.; Sato, T. Preparation and characterization of nitrogen doped $SrTiO_3$ photocatalyst. *J. Photochem. Photobiol., A* **2004**, *165*, 149–156.

(15) Ishii, T.; Kato, H.; Kudo, A. H_2 evolution from an aqueous methanol solution on $SrTiO_3$ photocatalysts codoped with chromium and tantalum ions under visible light irradiation. *J.Photochem. Photobiol., A* **2004**, *163*, 181–186.

(16) Martin, C.; Solanl, G.; Rives, V.; Marci, G.; Palmisano, L.; Sclafani, A. Physico-chemical properties of WO_3/TiO_2 systems employed for 4-nitrophenol photodegradation in aqueous medium. *Catal. Lett.* **1997**, *49*, 235–243.

(17) Takeuchi, T.; Tani, T.; Satoh, T. Microcomposite particles $Sr_3Ti_2O_7$ - $SrTiO_3$ with an epitaxial core-shell structure. *Solid State Ionics* **1998**, *108*, 67–71.

(18) Kubo, T.; Nozoye, H. Surface structure of $SrTiO_3$(1 0 0). *Surf. Sci.* **2003**, *542*, 177–191.

(19) Sudoh, K.; Iwasaki, H. Step distribution on vicinal $SrTiO_3$(0 0 1) surfaces. *Surf. Sci.* **2004**, *557*, 151–155.

(20) Ling, H. C.; Yan, M. F. Second phase development in Sr-doped TiO_2. *J. Mater. Sci.* **1983**, *18*, 2688–2696.

(21) Zhou, J.; Zhang, Y.; Zhao, X. S.; Ray, A. K. Photodegradation of benzoic acid over metal-doped TiO_2. *Ind. Eng. Chem. Res.* **2006**, *45*, 3503–3511.

(22) Farantos, S. C.; Filippou, E.; Stamatiadis, S.; Froudakis, G. E.; Muhlhauser, M.; Massaouti, M.; Sfounis, A.; Velegrakis, M. Photofragmentation spectra of Sr^+CO complex: Experiment and ab initio calculations. *Chem. Phys. Lett.* **2002**, *366*, 231–237.

(23) Sakthivel, S.; Neppolian, B.; Shankar, M. V.; Arabindoo, B.; Palanichamy, M.; Murugesan, V. Solar photocatalytic degradation of azo dye: Comparison of photocatalytic efficiency of ZnO and TiO_2. *J. Sol. Energy Mater. Cells* **2003**, *77*, 65–82.

Received for review July 27, 2009
Revised manuscript received December 25, 2009
Accepted December 29, 2009

IE901191Z